Chapter 12

Resonant Excitation of Plasmons in Bi-Gratings

Taikei Suyama, Akira Matsushima, Yoichi Okuno and Toyonori Matsuda

Additional information is available at the end of the chapter

http://dx.doi.org/10.5772/50754

1. Introduction

Metal gratings have an interesting property known as resonance absorption in the optics region [Raeter 1982], which causes partial or total absorption of incident light energy. This absorption is associated with the resonant excitation of plasmons on a grating surface; incident light couples with surface plasmons via an evanescent spectral order generated by the grating [Nevière 1982]. Resonance absorption in metal film gratings has been the subject of many theoretical [Nevière 1982] and experimental investigations focused on various applications including chemical sensing [DeGrandpre 1990, Zoran 2009], surface enhanced phenomena such as Raman scattering [Nemetz 1994], and photonic bandgaps [Barnes 1995, Tan 1998].

A thin-film metal grating, which is a corrugated thin metal film, also results in absorption similar to that observed for thick gratings [Inagaki, Motosuga 1985, Chen 2008, Bryan-Brown 1991, Davis 2009]. Absorption in thin-film metal gratings, however, is much more complicated than in thick gratings because of the existence of coupled plasmon modes in addition to those observed in thick gratings. If the metal film is sufficiently thick, single-interface surface plasmons (SISPs) alone are excited [Raeter 1977, Okuno 2006, Suyama 2009]. However, if the film is sufficiently thin, simultaneous excitation of surface plasmons occurs on both surfaces; these plasmons interfere with each other and produce two coupled plasmon modes, short-range surface plasmons (SRSPs) and long-range surface plasmons (LRSPs) [Chen 1988, Hibbins 2006].

Most previous studies on resonance absorption have mainly dealt with metal gratings whose surfaces are periodic in one direction. Metal bi-gratings, which are periodic in two directions, also yield plasmon resonance absorption, similar to singly periodic gratings [Glass 1982, Glass 1983, Inagaki, Goudonnet 1985, Harris 1996]. In this work, we therefore investigated coupled plasmon modes excited in multilayered bi-gratings [Matsuda 1993, Matsuda 1996, Suyama 2010]. We anticipated interesting behavior in the resonance

phenomenon due to the presence of the double periodicity. Further, in view of the fact that layered gratings are interesting structures for optical device applications, we investigated a multilayered bi-gratings, which is a stack of thin-film bi-gratings made of a dielectric or metal. This paper is structured as follows. After formulating the problem in Section **2**, we briefly describe a method for obtaining a solution in Section **3**. Focusing our attention on the resonant excitation of plasmon modes, we then show the computational results in Section **4**, before presenting the conclusions of this study.

2. Formulation of the problem

Here, we formulate the problem of diffraction from multilayered bi-gratings when an electromagnetic plane wave is incident on it. The time-dependent factor, $\exp(-i\omega t)$, is suppressed throughout this paper as customary.

2.1. Geometry of the gratings

Figure 1 shows the schematic representation of multilayered sinusoidal gratings with double periodicity. The grating, with L-1 laminated grating layers, has a period d in both the X- and Y-directions. The semi-infinite regions corresponding to the medium above the

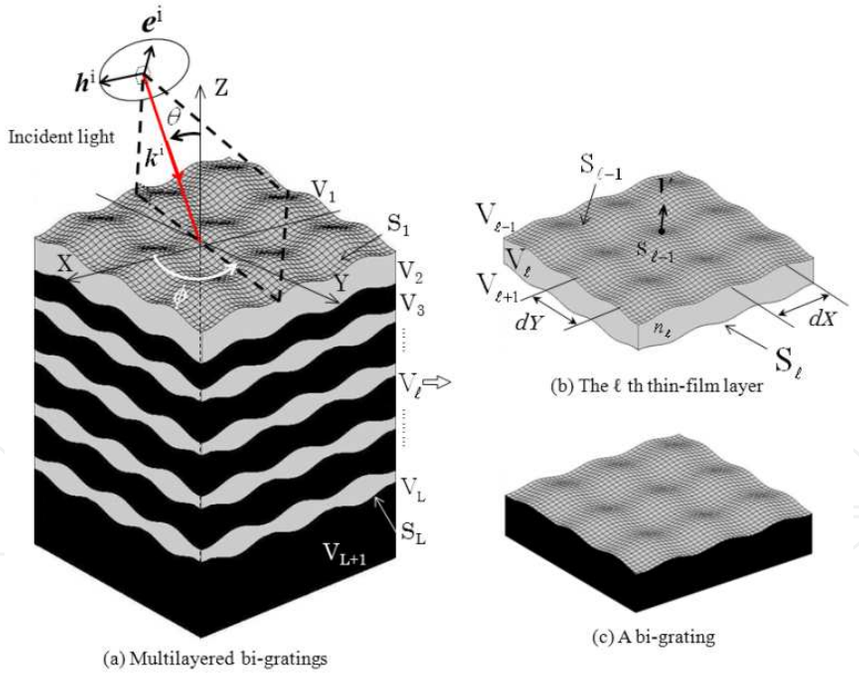

Figure 1. Schematic representation of bi-gratings. (a) Multilayered bi-gratings; (b) The l th thin-film bi-grating; (c) A bi-grating

grating and the substrate are denoted by V_1 and V_{L+1}, respectively. The individual layers in the grating, beginning from the upper layer (light-incidence side), are denoted by $V_\ell\left(\ell=2,3,\ldots,L\right)$. All of the regions $V_\ell\left(\ell=1,2,\ldots,L+1\right)$ are filled with isotropic and homogeneous media with refractive indices n_ℓ, and the permeability of each region is equal

to that of vacuum, μ_0. The interface between V_ℓ and $\mathrm{V}_{\ell+1}$ is denoted by S_ℓ ($\ell = 1,2,\ldots,L$). The profile of S_ℓ is sinusoidal and is given by

$$z = \eta_\ell(x,y) = \frac{h_l}{4}\left\{\sin\left(\frac{2\pi x}{d} + p_\ell\right) + \sin\left(\frac{2\pi y}{d} + p_\ell\right)\right\} - \sum_{i=1}^{\ell-1} e_i \tag{1}$$

Here, p_ℓ represents the phase of S_ℓ in each direction, and e_ℓ denotes the average distance between S_ℓ and S_{l+1}. The value h_ℓ is regarded as the groove depth of the boundary S_ℓ.

It should be noted that we can easily generalize the shape of S_ℓ by distinguishing between d and p_ℓ in the X-and Y-directions, by writing them as d_x, d_y, $p_{x\ell}$ and $p_{y\ell}$, respectively. A singly periodic grating is a special case where $d_y \to \infty$ in the doubly periodic case. In the present paper, we concentrate our attention on describing the analysis only for the doubly periodic case, since it reduces to the singly periodic case through a simple procedure.

2.2. Incident wave

The electric and magnetic fields of an incident wave are given by

$$\begin{pmatrix} E^{\mathrm{i}} \\ H^{\mathrm{i}} \end{pmatrix}(P) = \begin{pmatrix} e^{\mathrm{i}} \\ h^{\mathrm{i}} \end{pmatrix} \exp\left(ik^{\mathrm{i}} \cdot P \right) \tag{2}$$

with

$$\boldsymbol{h}^{\mathrm{i}} = \left(1/\omega\mu_0\right)\boldsymbol{k}^{\mathrm{i}} \times \boldsymbol{e}^{\mathrm{i}} \tag{3}$$

Here, P is the position vector for an observation point P(X, Y, Z), and $\boldsymbol{k}^{\mathrm{i}}$ is the wave vector of the incident wave defined by

$$\boldsymbol{k}^{\mathrm{i}} = \left[\alpha, \beta, -\gamma\right]^{\mathrm{T}} \tag{4}$$

where $\alpha = n_0 k \sin\theta\cos\varphi$, $\beta = n_0 k \sin\theta\sin\varphi$, and $\gamma = n_0 k \cos\theta$. The symbol k (= $2\pi/\lambda$) is the wave number in vacuum and λ is the wavelength of the incident wave. We define θ and φ as polar and azimuth angles, respectively, as shown in Fig. 1(a), and the superscript "T" denotes a transposition.

The amplitude of the incident electric field can be decomposed into TE and TM modes [Chen 1973] (with respect to the Z-axis) and is written as

$$\boldsymbol{e}^{\mathrm{i}} = \cos\delta\,\boldsymbol{e}^{\mathrm{TE}} + \sin\delta\,\boldsymbol{e}^{\mathrm{TM}} \tag{5}$$

$$\boldsymbol{e}^{\mathrm{TE}} = \left[\sin\varphi, -\cos\varphi, 0\right]^{\mathrm{T}} \tag{6}$$

$$\boldsymbol{e}^{\mathrm{TM}} = \left[\cos\theta\cos\varphi, \cos\theta\sin\varphi, \sin\theta\right]^{\mathrm{T}} \tag{7}$$

Here, the superscript TE (TM) indicates the absence of a Z component of the electric (magnetic) field.

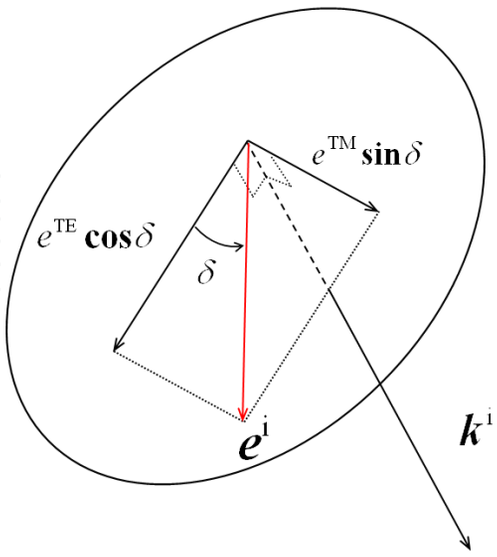

Figure 2. Definition of a polarization angle.

The symbol δ is the polarization angle between $\boldsymbol{e}^{\mathrm{TE}}$ and $\boldsymbol{e}^{\mathrm{i}}$ as shown in Fig. 2; for $\delta = 0^\circ$ ($\delta = 90^\circ$), this represents TE-mode (TM-mode) incidence.

2.3. Diffracted wave

We denote the diffracted fields as $E_\ell(P)$ and $H_\ell(P)$ in the region $V_\ell(\ell = 1,2,\ldots L, L+1)$. These satisfy the following conditions:

(C1) Helmholtz equation:

$$\left(\nabla^2 + n_\ell^2 k_\ell^2\right)\begin{pmatrix}\boldsymbol{E}_\ell \\ \boldsymbol{H}_\ell\end{pmatrix}(\boldsymbol{P}) = 0 \quad (\ell = 1,2,\ldots L, L+1) \tag{8}$$

(C2) Radiation conditions:

E_1 and H_1 propagate or attenuate in the positive Z-direction.

E_{L+1} and E_{L+1} propagate or attenuate in the negative Z-direction.

(C3) Periodicity conditions:

$$f(X+d, Y, Z) = \exp(i\alpha d) f(X, Y, Z) \tag{9}$$

$$f(X, Y+d, Z) = \exp(i\beta d) f(X, Y, Z) \tag{10}$$

Here, f denotes any component of $E_\ell(P)$ or $H_\ell(P)$.

(C4) Boundary condition ($0 < X < d$; $0 < Y < d$; $\ell = 1,2,...,L$):

$$\boldsymbol{v}\times\left[\begin{pmatrix}\boldsymbol{E}_{\ell-1}\\ \boldsymbol{H}_{\ell-1}\end{pmatrix}+\delta_{\ell 1}\begin{pmatrix}\boldsymbol{E}^{\mathrm{i}}\\ \boldsymbol{H}^{\mathrm{i}}\end{pmatrix}-\begin{pmatrix}\boldsymbol{E}_{\ell}\\ \boldsymbol{H}_{\ell}\end{pmatrix}\right]=0\quad(\text{on }\boldsymbol{S}_{\ell}) \tag{11}$$

where $\delta_{\ell 1}$ is the Kronecker delta, and ν_{ℓ} denotes the unit vector normal to the surface S_{ℓ}, which is given by

$$\nu_{\ell}=\frac{\left[-\dfrac{\partial\eta_{\ell}(X,Y)}{\partial X},-\dfrac{\partial\eta_{\ell}(X,Y)}{\partial Y},1\right]}{\sqrt{\left(\dfrac{\partial\eta_{\ell}(X,Y)}{\partial X}\right)^{2}+\left(\dfrac{\partial\eta_{\ell}(X,Y)}{\partial Y}\right)^{2}+1}} \tag{12}$$

3. Mode-matching method

We next explain the mode-matching method [Yasuura 1965, Yasuura 1971, Okuno 1990] for determining the diffracted field produced by the multilayered bi-grating. We introduce vector modal functions in the region $V_{\ell}(\ell=1,...,\mathrm{L}+1)$ to express the diffracted field in each individual region. To construct the wave functions $E_{\ell N}^{\mathrm{d}}(\boldsymbol{P})$ and $H_{\ell N}^{\mathrm{d}}(\boldsymbol{P})$, we define the electric modal function $\phi_{\ell mn}^{\mathrm{TE,TM}\pm}(\boldsymbol{P})$ and the magnetic modal function $\psi_{\ell mn}^{\mathrm{TE,TM}\pm}(\boldsymbol{P})$ as

$$\varphi_{\ell mn}^{\mathrm{TE,TM}\pm}(\boldsymbol{P})=e_{\ell mn}^{\mathrm{TE,TM}\pm}\phi_{\ell mn}^{\pm}(\boldsymbol{P}) \tag{13}$$

$$e_{\ell mn}^{\mathrm{TE}\pm}=\frac{k_{\ell mn}^{\pm}\times i_{Z}}{\left|k_{\ell mn}^{\pm}\times i_{Z}\right|},\ e_{\ell mn}^{\mathrm{TM}\pm}=\frac{e_{\ell mn}^{\mathrm{TE}\pm}\times k_{\ell mn}^{\pm}}{\left|e_{\ell mn}^{\mathrm{TE}\pm}\times k_{\ell mn}^{\pm}\right|} \tag{14}$$

$$\psi_{\ell mn}^{\mathrm{TE,TM}\pm}(\boldsymbol{P})=\frac{1}{\omega\mu_{0}}k_{\ell mn}^{\pm}\times\varphi_{\ell mn}^{\mathrm{TE,TM}\pm}(\boldsymbol{P}) \tag{15}$$

where $\phi_{\ell mn}^{\pm}(\boldsymbol{P})$ is the solution of the Helmholtz equation satisfying the periodic condition in the region $V_{\ell}(\ell=1,.2,..,L+1)$. It is written as

$$\varphi_{\ell mn}^{\pm}(\boldsymbol{P})=\exp\left(ik_{\ell mn}^{\pm}\cdot\boldsymbol{P}\right)\quad(m,n=0,\pm1,\pm2,...) \tag{16}$$

where the positive and negative signs match on either side of the equation, and $k_{\ell mn}^{\pm}$ is the wave vector of the (m,n)th order diffracted wave given by

$$k_{\ell mn}^{\pm}=\left[\alpha_{m},\beta_{n},\pm\gamma_{\ell mn}\right]^{\mathrm{T}} \tag{17}$$

$$\alpha_{m}=\alpha+\frac{2m\pi}{d},\ \beta_{n}=\beta+\frac{2n\pi}{d} \tag{18}$$

$$\gamma_{\ell mn} = \left(n_\ell^2 k^2 - \alpha_m^2 - \beta_n^2\right)^{1/2},\ \mathrm{Re}\left(\gamma_{\ell mn}\right) \geq 0 \text{ and } \mathrm{Im}\left(\gamma_{\ell mn}\right) \geq 0 \tag{19}$$

Note that the superscripts + and - represent upwardly and downwardly propagating waves in the positive and negative Z-direction, respectively.

In terms of the linear combinations of the vector modal functions, we form approximate solutions for the diffracted electric and magnetic fields in V_ℓ :

$$\begin{aligned}\begin{pmatrix} \boldsymbol{E}_{\ell N}^{\mathrm{d}} \\ \boldsymbol{H}_{\ell N}^{\mathrm{d}} \end{pmatrix}(\boldsymbol{P}) = &\sum_{m,n=-N}^{N} A_{\ell mn}^{\mathrm{TE}+}(N) \begin{pmatrix} \varphi_{\ell mn}^{\mathrm{TE}+} \\ \psi_{\ell mn}^{\mathrm{TE}+} \end{pmatrix}(\boldsymbol{P}) \\ &+ \sum_{m,n=-N}^{N} A_{\ell mn}^{\mathrm{TM}+}(N) \begin{pmatrix} \varphi_{\ell mn}^{\mathrm{TM}+} \\ \psi_{\ell mn}^{\mathrm{TM}+} \end{pmatrix}(\boldsymbol{P}) \\ &+ \sum_{m,n=-N}^{N} A_{\ell mn}^{\mathrm{TE}-}(N) \begin{pmatrix} \varphi_{\ell mn}^{\mathrm{TE}-} \\ \psi_{\ell mn}^{\mathrm{TE}-} \end{pmatrix}(\boldsymbol{P}) \\ &+ \sum_{m,n=-N}^{N} A_{\ell mn}^{\mathrm{TM}-}(N) \begin{pmatrix} \varphi_{\ell mn}^{\mathrm{TM}-} \\ \psi_{\ell mn}^{\mathrm{TM}-} \end{pmatrix}(\boldsymbol{P}) \\ &\left(\ell = 1,2,\ldots,L+1\right)\end{aligned} \tag{20}$$

with

$$\psi_{\ell mn}^{\mathrm{TE,TM}\pm}(\boldsymbol{P}) = \frac{1}{\omega\mu_0} k_{\ell mn}^{\pm} \times \phi_{\ell mn}^{\mathrm{TE,TM}\pm}. \tag{21}$$

Here, $A_{1mn}^{\mathrm{TE}-}(N) = A_{1mn}^{\mathrm{TM}-}(N) = 0$ and $A_{L+1mn}^{\mathrm{TE}+}(N) = A_{L+1mn}^{\mathrm{TM}+}(N) = 0$ because of the radiation conditions (C3) stated in **Section 2.3**.

The approximate solutions $\boldsymbol{E}_{\ell N}^{\mathrm{d}}(\boldsymbol{P})$ and $\boldsymbol{H}_{\ell N}^{\mathrm{d}}(\boldsymbol{P})$ already satisfy the Helmholtz equation (C1), the periodicity conditions (C2), and the radiation conditions (C3). The unknown coefficients $A_{\ell mn}^{\mathrm{TE}\pm}(N)$ and $A_{\ell mn}^{\mathrm{TM}\pm}(N)$ are therefore determined such that the solutions approximately satisfy the boundary conditions (C4). In the mode-matching method [Yasuura 1996, Yasuura 1971, Okuno 1990], the least-squares method is employed to fit the solution to the boundary conditions [Hugonin 1981]. That is, we find coefficients that minimize the weighted mean-square error by

$$\begin{aligned} I_N = &\int_{S_1'} \left| \nu \times \left[\mathrm{E}_{1N}^{\mathrm{d}} + \mathrm{E}^{\mathrm{i}} - \mathrm{E}_{2N}^{\mathrm{d}} \right](s_1) \right|^2 ds \\ &+ \left|\Gamma_1\right|^2 \int_{S_1'} \left| \nu \times \left[\mathrm{H}_{1N}^{\mathrm{d}} + \mathrm{H}^{\mathrm{i}} - \mathrm{H}_{2N}^{\mathrm{d}} \right](s_1) \right|^2 ds \\ &+ \sum_{\ell=2}^{L} \left\{ \int_{S_\ell'} \left| \nu \times \left[\mathrm{E}_{\ell N}^{\mathrm{d}} - \mathrm{E}_{\ell+1N}^{\mathrm{d}} \right](s_\ell) \right|^2 ds + \right. \\ &\left. \left|\Gamma_\ell\right|^2 \int_{S_\ell'} \left| \nu \times \left[\mathrm{H}_{\ell N}^{\mathrm{d}} - \mathrm{H}_{\ell+1N}^{\mathrm{d}} \right](s_\ell)^2 \right| ds \right\} \end{aligned} \tag{22}$$

Here, $S_\ell^{'}$ is a one-period cell of the interface S_ℓ, and Γ_ℓ is the intrinsic impedance of the medium in V_ℓ.

To solve the least-squares problem on a computer, we first discretize the weighted mean-square error I_N by applying a two-dimensional trapezoidal rule where the number of divisions in the *x*-and *y*-direction is chosen as 2(2*N* + 1) [Yasuura 1965, Yasuura 1971, Okuno 1990]. We then solve the discretized least-squares problem by the QR decomposition method. Computational implementation of the least-squares problem is detailed in the literature [Lawson 1974, Matsuda 1966, Suyama 2008].

4. Numerical results

Here we show some numerical results obtained by the method described in the preceding section. After making necessary preparation, we show the results for three the bi-grating, thin-film bi-grating and multilayered thin-film bi-gratings cases.

4.1. Preparation

It is known that the solutions obtained by mode-matching method [Yasuura 1965, Yasuura 1971, Okuno 1990] have proof of convergence. We, therefore, can employ the coefficient $A_{\ell mn}^{\mathrm{TM,TE}\pm}(N)$ with sufficiently large *N* for which the coefficients are stable in evaluating diffracted fields.

The power reflection and transmission coefficient of the (*m*, *n*) order propagating mode in V_1 and $\mathrm{V}_{\mathrm{L+1}}$ are given by

$$\rho_{\mathrm{mn}} = \rho_{mn}^{\mathrm{TE}} + \rho_{mn}^{\mathrm{TM}} \ [\mathrm{Re}(\gamma_{1mn}) \geq 0],\ \rho_{mn}^{\mathrm{TE}} = \frac{\gamma_{1mn}}{\gamma}\left|A_{1mn}^{\mathrm{TE+}}\right|^2,\ \rho_{mn}^{\mathrm{TM}} = \frac{\gamma_{1mn}}{\gamma}\left|A_{1mn}^{\mathrm{TM+}}\right|^2 \tag{23}$$

$$\tau_{\mathrm{mn}} = \tau_{mn}^{\mathrm{TE}} + \tau_{mn}^{\mathrm{TM}} \ [\mathrm{Re}(\gamma_{L+1mn}) \geq 0],\ \tau_{mn}^{\mathrm{TE}} = \frac{\gamma_{L+1mn}}{\gamma}\left|A_{L+1mn}^{\mathrm{TE-}}\right|^2,\ \tau_{mn}^{\mathrm{TM}} = \frac{\gamma_{L+1mn}}{\gamma}\left|A_{L+1mn}^{\mathrm{TM-}}\right|^2 \tag{24}$$

The coefficient defined above is the power carried away by propagating diffraction orders normalized by the incident power. We calculate the total diffraction efficiency $\rho^{\mathrm{total}} = \sum^{'} \rho_{mn}$ where $\sum^{'}$ denotes a summation over the propagating orders.

Although it is known that the solutions obtained by mode-matching modal expansion method [Yasuura 1965, Yasuura 1971, Okuno 1990] have proof of convergence for problems of diffraction by gratings, we compare our results with other existing theoretical [Glass 1983] and experimental results [Inagaki, Goudonnet 1985] on plasmon resonance absorption in bi-gratings to show the validity of the present method. Figure 3 shows the reflectivity curves calculated by the present method and those from Rayleigh's method [Glass 1983] for three sinusoidal silver bi-gratings with different corrugation amplitudes. As confirmed in Fig. 3, the reflectivity curves from the present method are coincident with those of the

Rayleigh's method [Glass 1983]. Next, we make comparison with the experimental results [Inagaki, Goudonnet 1985] in which the resonance angle θ_d, i.e., the polar angle at which the dip of reflectivity occurs, is observed near 55° for a sinusoidal silver bi-grating with h = 0.048 μm, d = 2.186 μm, λ = 0.633 μm, and ϕ = 45°. The resonance angle calculated from the present metod for these parameters is θ_d = 54.1°, which is close to the experimental data. These examples show that the present method gives reliable results for the analysis of plasmon-resonance absorption in metal bi-gratings.

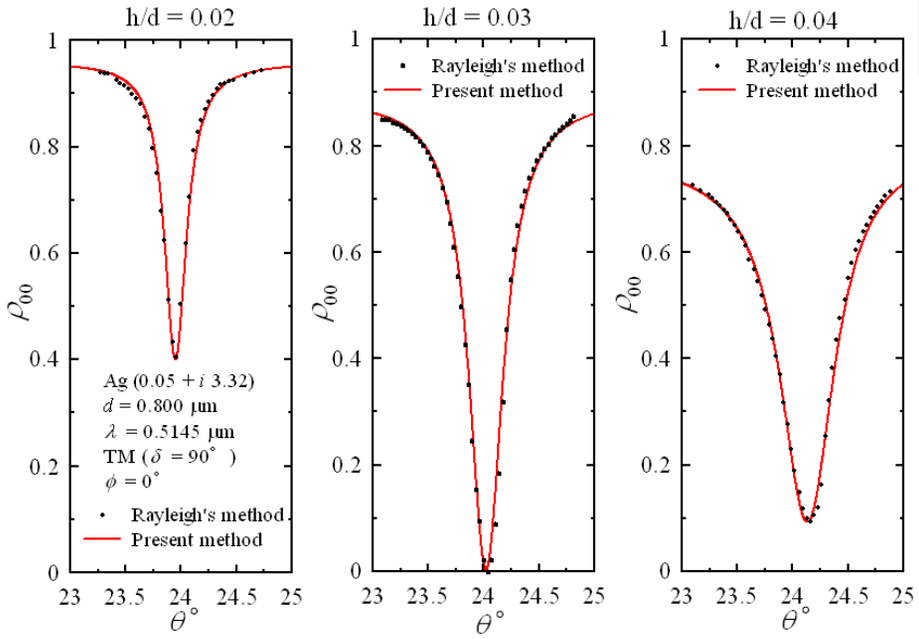

Figure 3. Comparison of resonance absorption curves calculated by the present method with other existing theoretical results. Solid curves show our results, and dotted curves are taken from Figure 2. of Ref. [Glass 1983].

In the numerical examples presented here, we deal with a shallow sinusoidal silver bi-grating with height h = 0.030 μm and period d = 0.556 μm. The wavelength of an incident light is chosen as λ = 0.650 μm. We take n_2 = 0.07+i4.20 as the refractive index of silver at this wavelength [Hass 1963].

It should be noted, however, that the index of a metal film depends not only on the wavelength but also on the thickness of the film, in particular when the film is extremely thin it may take unusual values if circumstances require. When dealing with a thin metal structure, hence, we should be careful in using the index value given in the literature. As for the value taken in our computation, we assume that n_2 = 0.07+i4.20 is available even for the case of e/d = 0.02. This is because a similar assumption was supported by experimental data in a problem of diffraction by an aluminum grating with a thin gold over-coating.

4.2. A bi-grating case

Using the numerical algorithm stated in the previous section, we first investigate the absorption in a metal bi-gratings by L = 1 as shown in Fig. 1(c). The semi-infinite regions

corresponding to the medium above the grating and the substrate are denoted by V_1 and V_2, respectively. V_1 is vacuum (V) with a relative refractive index n_1=1 and V_2 consists of a lossy metal characterized by a complex refractive index n_2.

4.2.1. Diffraction efficiency

Figure 4 shows the total diffraction efficiency of a sinusoidal silver bi-grating as functions of a polar angle θ when the azimuthal angle $\phi = 30^\circ$ is fixed. In the efficiency curves we observe four dips which occur at the same angles of incidence for both TE and TM polarized incident light. In this subsection, we demonstrate that the dips are associated with absorption that is caused by the coupling of surface plasmons with an evanescent mode diffracted by a sinusoidal bi-grating. For convenience, the four dips in Fig. 4 are labeled as A, B, C, and D.

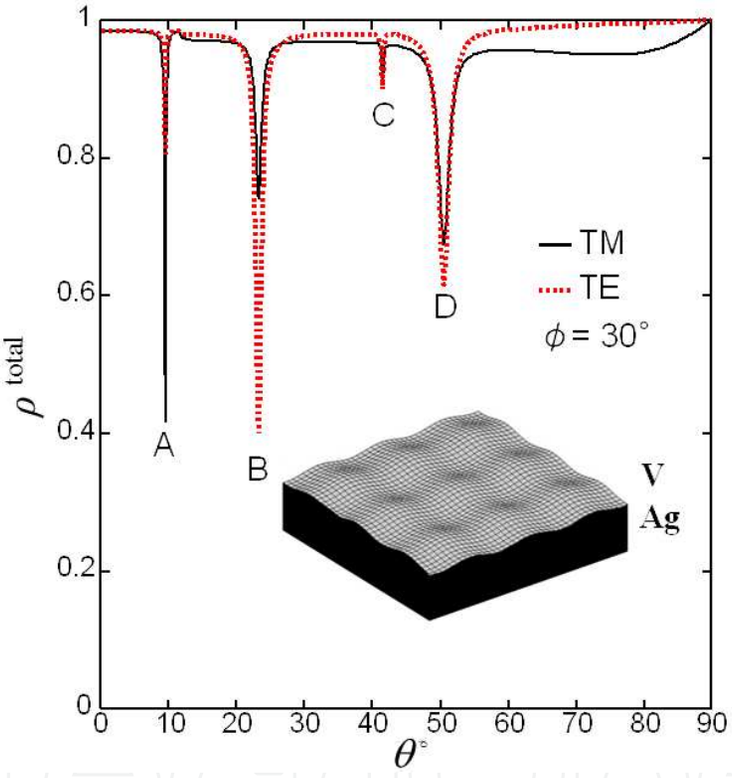

Figure 4. Total diffraction efficiencies ρ^{total} as functions of θ (L=1).

4.2.2. Expansion coefficients

In Fig. 5 we plot the expansion coefficients of the (0, -1)st-order and (-1, 0)th-order TM vector modal function, which are two evanescent modes, as a functions of θ under the same parameters as in Fig. 4. Solid curves in Fig. 5 represent the real part of the expansion coefficient, and dashed curves for the imaginary part. We observe a resonance curve of the expansion coefficient $A^{\text{TM}}_{1(-1,0)}$ at the angles of incidence $\theta = 9.5^\circ$, i.e., dip A, and $A^{\text{TM}}_{1(0,-1)}$ at the angles of incidence $\theta = 23.3^\circ$, 41.5° and 49.5°, i.e., dips B, C, and D in Fig. 4 for both TE and TM incidence.

This implies that the TM component of the (0, -1)st-order and (-1, 0)th-order evanescent mode couples with surface plasmons at dips B and D. We can similarly confirm that dips A and C are associated with the coupling of the TM component of the (-1, 0)th- and (-1, -1)st-order evanescent mode, respectively, with surface plasmons, although we do not include any numerical example here.

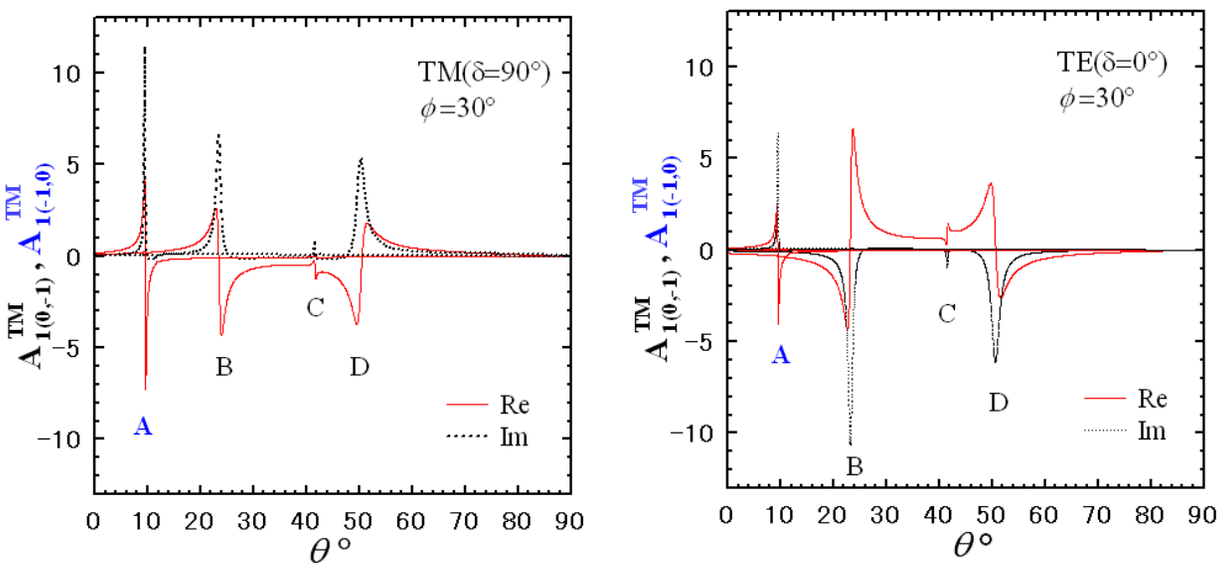

Figure 5. $A^{\mathrm{TM}}_{1(0,-1)}$ and $A^{\mathrm{TM}}_{1(-1,0)}$ as functions of θ for both TM- (a) and TE- (b) polarized incident light.

4.2.3. Field distributions and energy flows

In order to investigate the resonant excitation of surface plasmons, we study field distributions and energy flows in the vicinity of the grating surface when the absorption occurs. Here we consider the case of the dip B at which the TM component of the (0, -1)st-order evanescent mode couples with surface plasmons. We calculate the electric field of the TM component of the (0, -1)st-order evanescent mode $E^{\mathrm{TM}}_{\ell 0-1} = A^{\mathrm{TM}}_{\ell 0-1}(N)\ \varphi^{\mathrm{TM}}_{\ell 0-1}(\ell = 1,2)$ and the total electric field E^{t}. The magnitude of these fields along the Z-axis where $\mathrm{Y} = (\beta_{-1}/\alpha_0) * \mathrm{X}$ is plotted in Fig. 6(a). We observe in this figure that very strong electric fields are induced at the grating metal surface and the fields exponentially decay away from the surface.

Next we show the energy flows **S** that are the real part of Poynting's vectors for the total field. The X and Y components of the energy flows **S** are plotted as the vector (S_X, S_Y) in Fig. 6(b). The energy flows are calculated over the region close to the grating surface:

$$\{\mathrm{P}(x,y,z): 0 \le x \le d, 0 \le y \le d, \\ z = (h/4)[\sin(2\pi \mathrm{x}/d) + \sin(2\pi y/d)] + 0.01d\}. \tag{25}$$

The energy flow at a point P is given by Re[$S(P)$], where $S(P)$=(1/ 2) $E^{\mathrm{t}}(P)\times H^{\mathrm{t}}(P)$ stands for Poynting's vector, E^{t} and H^{t} denote total fields, and the over-bar means complex conjugate.

We calculate the energy flow at each point located densely near the grating surface and show the results in Fig. 6(b).

Figure 6(b) shows that the energy of electromagnetic fields in the vicinity of the grating surface flows uniformly in the direction that the (0, -1)st-order evanescent mode travels in the XY plane. We thus confirm that surface plasmons are excited on the grating surface through the coupling of the TM component of an evanescent mode.

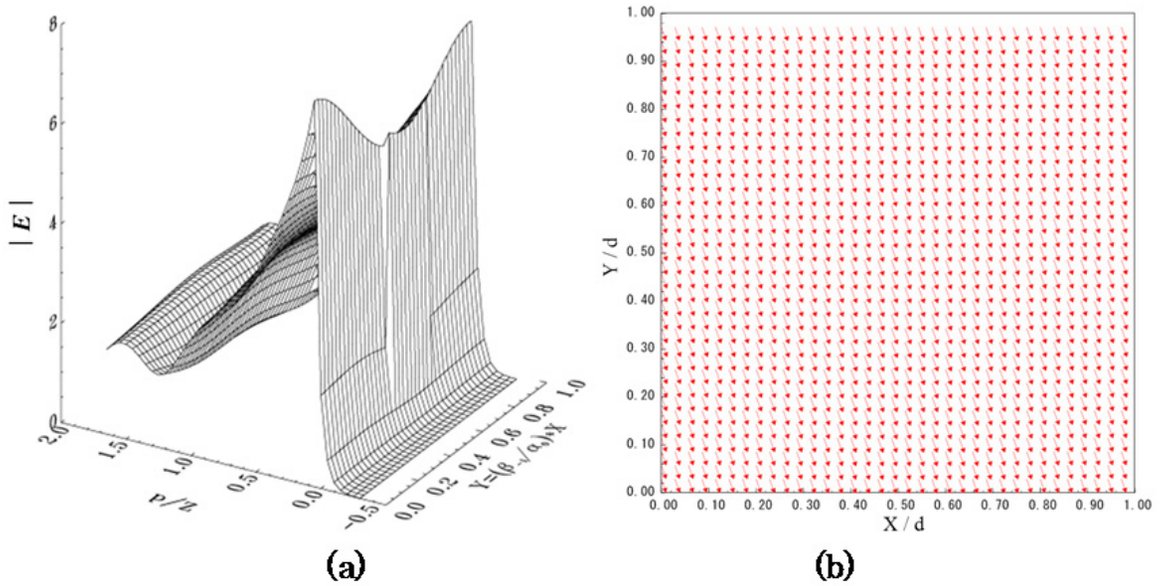

Figure 6. Field distribution (a) and Energy flow (b) for the total field when plasmon resonance absorption occurs at $\phi = 30^{\circ}$, $\theta = 23.3^{\circ}$.

4.2.4. Polarization conversion through plasmon resonance absorption

Diffracted fields from a sinusoidal metal bi-grating have both TE and TM component for an arbitrary polarized incident light. We therefore observe polarization conversion that a TM (or TE) component of the incident light is converted into a TE (or TM) component of the reflected light. It has been pointed out [Chen 1973, Inagaki, Goudonnet 1985] that the polarization conversion [Elston 1991, Matsuda 1999, Suyama 2007] is strongly enhanced when the plasmon-resonance absorption occurs in a sinusoidal metal bi-grating. Our study confirms the enhancement of polarization conversion through plasmon-resonance absorption. In Fig. 7, the TE and TM component of the diffraction efficiency ρ_{00} ($\rho_{00} = \rho_{00}^{\mathrm{TE}} + \rho_{00}^{\mathrm{TM}}$) of Fig. 4 are shown for the case of the TM incidence. The TM component ρ_{00}^{TM} is decreased at the position of the plasmon-resonance absorption, but the TE component ρ_{00}^{TE} is contrary increased there. That is, the resonant excitation of surface plasmons causes the enhancement of polarization conversion. On the other hand, in the case of the TE incidence the conversion from a TE to a TM component occurs through the plasmon-resonance absorption. It should be noted that the conversion efficiency depends on the azimuthal angle φ and the depth of the grating surface h.

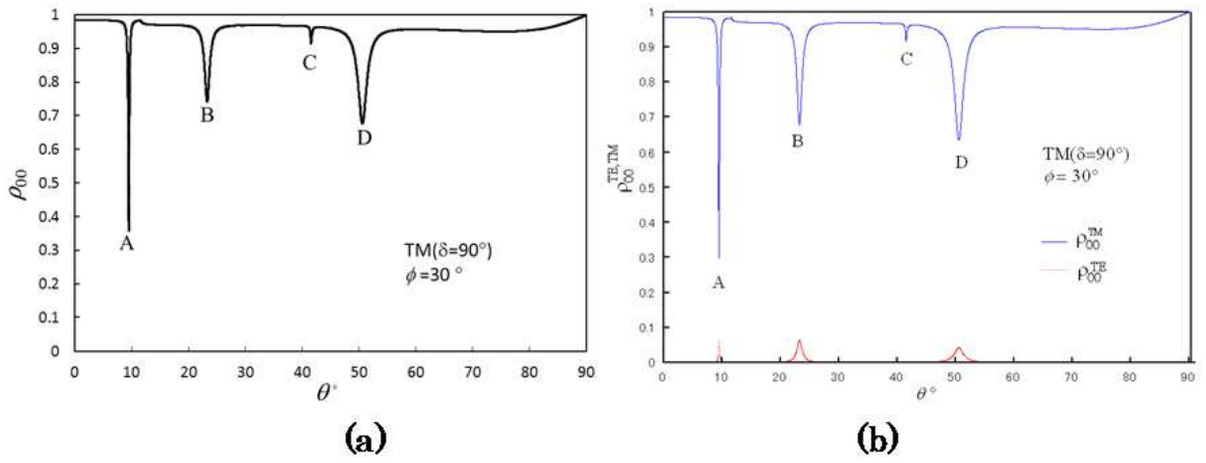

Figure 7. Diffraction efficiencies of ρ_{00} (a) ρ_{00}^{TE} and ρ_{00}^{TM} (b) as functions of θ; parameters are the same as in Figure 4.

4.2.5. Prediction of resonance angles

We seek to determine a complex incidence angle θ_c for which total or partial absorption occurs, i.e., $\rho_{\mathrm{total}}\ (=\rho_{00})$ takes a minimum. This angle relates to the propagation constant of the surface plasmon on the corrugated surface. Here, we denote by $\hat{\alpha}_{\mathrm{SP}}$ and $\hat{\beta}_{\mathrm{SP}}$ the X and Y components of the surface plasmon wave vector normalized by the wave number k_1:

$$\begin{aligned}\hat{\alpha}_{SP} &= \sin\theta_{\mathrm{c}}\cos\phi + m\lambda/d,\\ \hat{\beta}_{SP} &= \sin\theta_{\mathrm{c}}\sin\phi + n\lambda/d.\end{aligned} \tag{26}$$

In reality, we cannot realize a complex incidence angle θ_{c}. We can, however, estimate the real angle of incidence at which the absorption occurs by taking the real part of Eq. (26).

If the wavevector of the surface plasmon ($\hat{\alpha}_{\mathrm{SP}}$, $\hat{\beta}_{\mathrm{SP}}$) is obtained, we can estimate the resonance angle θ_{SP} for each azimuthal angle φ from the phase-matching condition for coupling of a surface plasmon wave with the (m, n)th-order evanescent mode:

$$\begin{aligned}\mathrm{Re}\{\hat{\alpha}_{\mathrm{SP}}\} &= \sin\theta_{\mathrm{SP}}\cos\varphi + m\lambda/d,\\ \mathrm{Re}\{\hat{\beta}_{\mathrm{SP}}\} &= \sin\theta_{\mathrm{SP}}\sin\varphi + n\lambda/d.\end{aligned} \tag{27}$$

We solve the homogenous problem [Nevière 1982] for a sinusoidal metal bi-grating by present method and then obtain the surface-plasmon wave vector. Table 1 shows the propagation constants of the surface plasmon and the resonance angles θ_{SP}. The data demonstrate that the estimated resonance angle θ_{SP} agrees with θ_{d} which is the absorption peak in Fig. 4. Figure 8 shows the estimated resonance angle θ_{SP} as a function of the azimuthal angle φ for the sinusoidal bi-grating considered in Fig. 4. Note that points A, B, C, and D in Fig. 8 are results obtained from the absorption peak of total-efficiency curves in Fig. 4. From this figure, we can find the resonance angle for each azimuthal angle.

Dip	Mode	Re($\hat{\alpha}_{SP}$)	Im($\hat{\alpha}_{SP}$)	Re($\hat{\beta}_{SP}$)	Im($\hat{\beta}_{SP}$)	θ°_{SP}	θ°_{d}
A	(-1, 0)	-1.026277	-0.000804	0.087099	-0.001279	9.49	9.5
B	(0, -1)	0.343795	-0.004910	-0.971021	-0.002498	23.39	23.3
C	(0, -1)	-0.595897	-0.001282	-0.837168	-0.000549	41.44	41.5
D	(0, -1)	0.668265	-0.004365	-0.778336	-0.005224	50.50	50.5
E	(0, -1)	0.149639	-0.000679	-1.019425	-0.000679	12.22	12.2
	(-1, 0)	-1.019426	-0.000679	0.149639	-0.000679	12.22	

[a] $h = 0.03\mu m$, $d = 0.556\mu m$, $\lambda = 0.650\mu m$

Table 1. Propagation Constants and Estimated Resonance Angles[a]

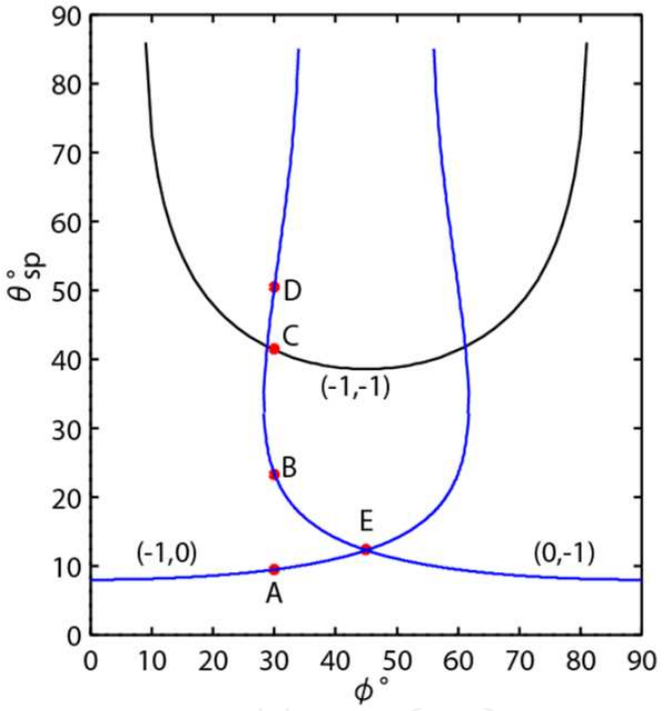

Figure 8. Resonance angles θ_{SP} as functions of azimuthal angle ϕ.

4.2.6. Simultaneous resonance absorption

From Fig. 8, it is predicted the angle of incidence at which the simultaneous resonance absorption occurs from the position of the intersection of the (-1,0) and (0,-1) curve. At the intersection **E**, the (0,-1)st- and (-1,0)th-order evanescent modes couple simultaneously with two surface-plasmon waves at the same angle of incidence. Thus, two surface-plasmon waves are excited simultaneously in directions symmetric with respect to the plane of incidence and interact with each other. The interference of the surface-plasmon waves causes the standing wave in the vicinity of the grating surface. This is confirmed from Figs. 9, the strong fields along the Z-axis where Y=X, and where the X and Y components of Poynting's vectors **S** on a surface $0.01d$ above the one-unit cell of the grating surface are

plotted as the vector (S_X, S_Y). We further observe in Fig. 10 that the simultaneous excitation of the surface plasmons waves causes the strong absorption for both TE- and TM-polarized incident light.

It has been reported [Barnes 1995, Ritchie 1968] that surface-plasmon band gaps exist at the angles of incidence at which simultaneous excitation of plasmon waves occurs, and that the appearance of the band gaps depends strongly on the surface profile. Hence, there is a possibility that a band gap will be observed at the point *E* in Figs. 9 and 10 provided that the grating profile is appropriately chosen, because two plasmon modes are excited at that point.

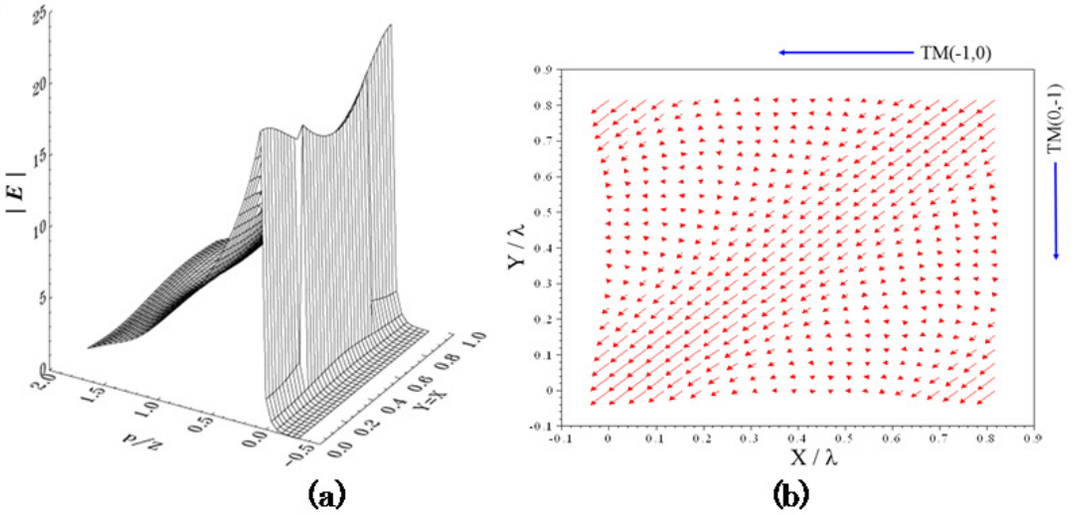

Figure 9. Field distributions and Energy flows for the total field when plasmon resonance absorption occurs.

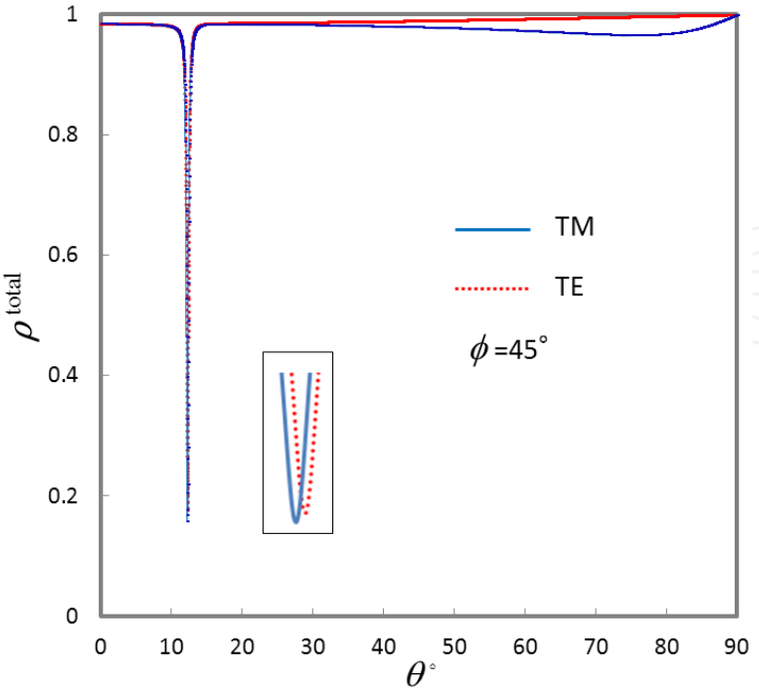

Figure 10. Total diffraction efficiencies ρ^{total} as functions of θ.

4.3. A Thin-film Bi-grating case

As a numerical example, we consider a sinusoidal silver (Ag) film bi-grating having a common period as shown in Fig. 1(b). The values of the parameters are the same as those in Fig. 4 except for the thickness of the silver film. Using the present algorithm, we calculated the diffraction efficiencies and field distributions to clarify the properties of the coupled surface plasmon modes.

4.3.1. Diffraction efficiency

First, we consider a sinusoidal silver-film bi-grating. The bi-grating is denoted by L = 2 (V/Ag/V). Figure 11 shows the (0,0)th order power reflection ρ_{00} in V_1 (Vacuum) (a) and the transmission coefficient τ_{00} in V_3 (Vacuum) (b) as functions of the incident angle θ for two values of e/d when the azimuth angle $\phi = 0^\circ$ is fixed; e is the thickness of the silver film. We observe partial absorption of the incident light as dips in the efficiency curves in Fig. 11(a), in addition to the constant absorption corresponding to the reflectivity of silver. We assume that the dips are caused by resonant excitation of surface plasmons. If this is the case, each of the dips can be related to one of the three types of plasmon modes: a SISP that is observed as a single dip at $\theta = 8.0^\circ$ on the $e/d = 0.4$ curve, and a SRSP and LRSP corresponding to the dips in the $e/d = 0.08$ curve at $\theta = 6.54^\circ$ and 8.8°, respectively.

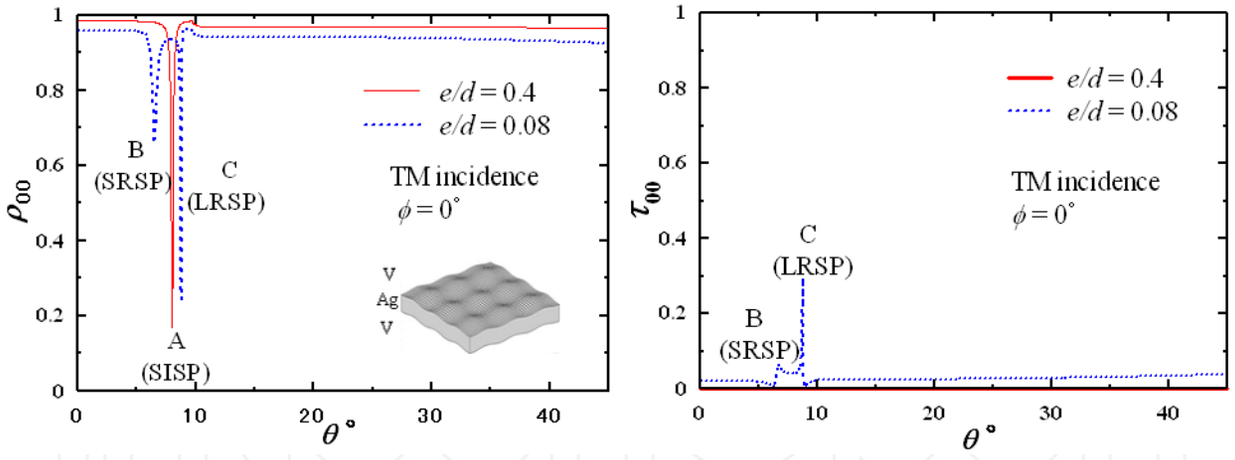

Figure 11. The (0, 0)-th order diffraction efficiencies ρ_{00} (a) and τ_{00} (b) as functions of θ for two values of e/d (L=2).

When the grating is thick ($e/d = 0.4$), the power can be seen in V_1 alone and no transmitted power exists in V_3 in Fig. 11. Increasing θ from 0°, we first observe the dip at $\theta = 8.0^\circ$ corresponding to absorption in Fig. 11(a). If the grating is relatively thin ($e/d = 0.08$), the power exists in both V_1 and V_3. Although the power in V_3 is generally small, it becomes large at the incidence angles for which absorption was observed in Fig. 11. This suggests that coupled oscillations occur on the upper and lower surfaces of the grating.

4.3.2. Expansion coefficients

We examined the same phenomena observing the modal expansion coefficients in $V_l (l = 1,3)$. Figures 12 and 13 illustrate the (-1,0)th-order coefficients $A^{TM+}_{1(-1,0)}$ for $e/d = 0.4$ and 0.08, respectively. We observe, in Fig. 12(a) ($e/d = 0.4$), the resonance characteristics (enhancement and rapid change in phase) of the coefficient $A^{TM+}_{1(-1,0)}$ near $\theta = 8.0^\circ$. The coefficient $A^{TM-}_{3(-1,0)} = 0$ remains unchanged, as seen in Fig. 12(b). This means that the incident wave illuminating the grating at this angle causes coupling between the (-1,0)th-order evanescent mode and some oscillation excited on the upper surface of the grating. The oscillation exists locally in the vicinity of the illuminated surface and hence does not have any influence on the field in V_3.

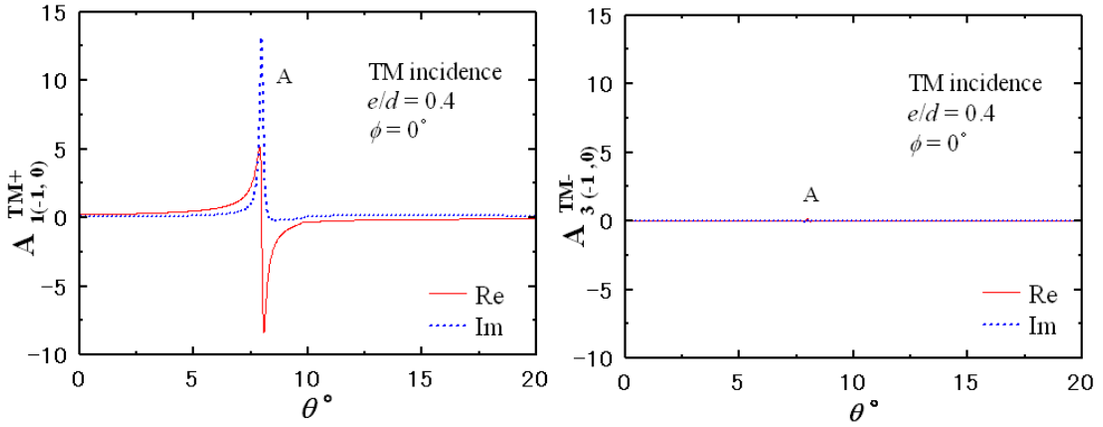

Figure 12. The (-1, 0)th order modal coefficients $A^{TM+}_{1(-1,0)}$ (a) and $A^{TM-}_{3(-1,0)}$ (b) as functions of θ at $e/d = 0.4$.

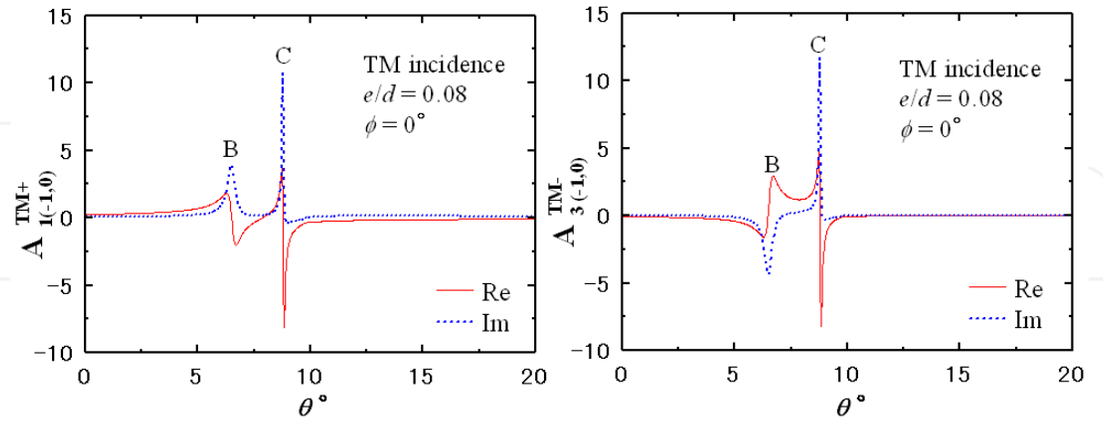

Figure 13. The (-1, 0)th order modal coefficients $A^{TM+}_{1(-1,0)}$ (a) and $A^{TM-}_{3(-1,0)}$ (b) as functions of θ at $e/d = 0.08$.

In Fig. 13 ($e/d = 0.08$), we find the resonance characteristics in both $A^{TM+}_{1(-1,0)}$ and $A^{TM-}_{3(-1,0)}$. In addition, they appear around two incidence angles: $\theta = 6.54^\circ$ and $\theta = 8.8^\circ$. This means that

the oscillation in the vicinity of the upper surface causes another oscillation on the lower surface at this thickness. The oscillations interfere with each other and result in two coupled oscillating modes: the SRSP and LRSP. This means that the TM component of the (-1,0)th order evanescent mode couples with the surface plasmons simultaneously excited on the upper and lower surface of the film grating. The two surface plasmons interfere with each other and result in symmetric and antisymmetric coupled modes, SRSP and LRSP, as we will see next.

4.3.3. Field distributions and energy flows

We consider the same phenomena observing the field distributions and energy flows near the grating surfaces. In the former we find that the total field is enhanced. In the latter we observe the symmetric (even) and anti-symmetric (odd) nature of the oscillations, which correspond to the LRSP and SRSP [Raeter 1977].

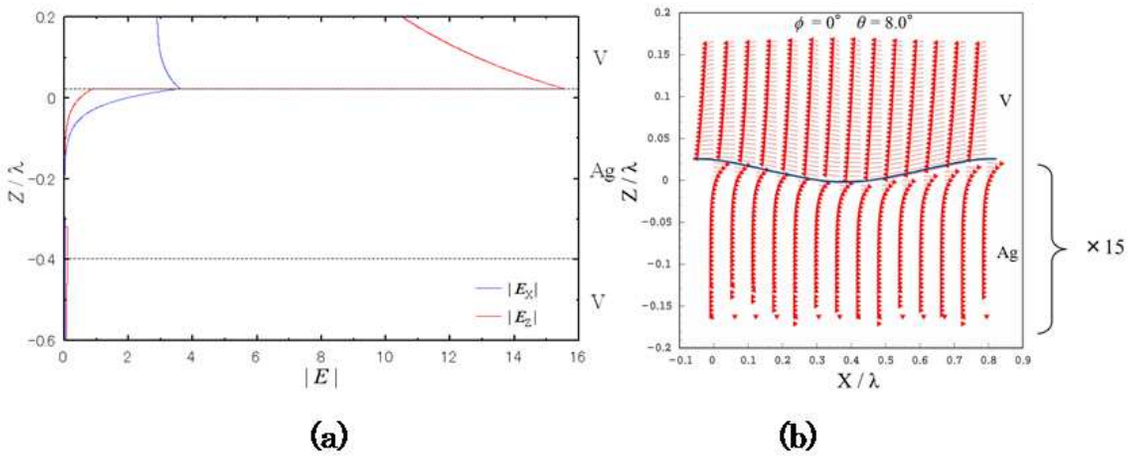

Figure 14. Field distributions (a) and energy flows (b) at $\theta = 8.0^{\circ}$, which corresponds to the single dip on the $e/d = 0.4$ curve in Fig. 11.

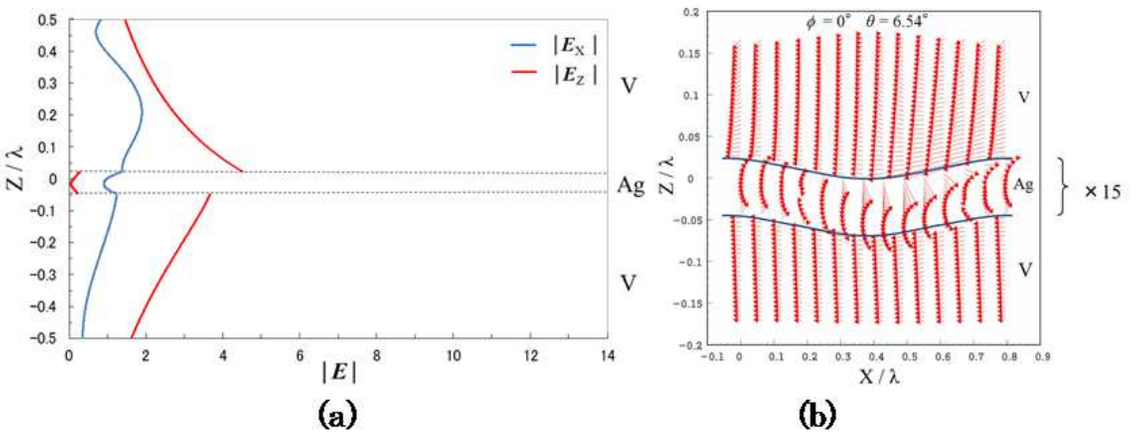

Figure 15. Field distributions (a) and energy flows (b) at $\theta = 6.54^{\circ}$, which corresponds to the left dip on the $e/d = 0.08$ curve in Fig. 11.

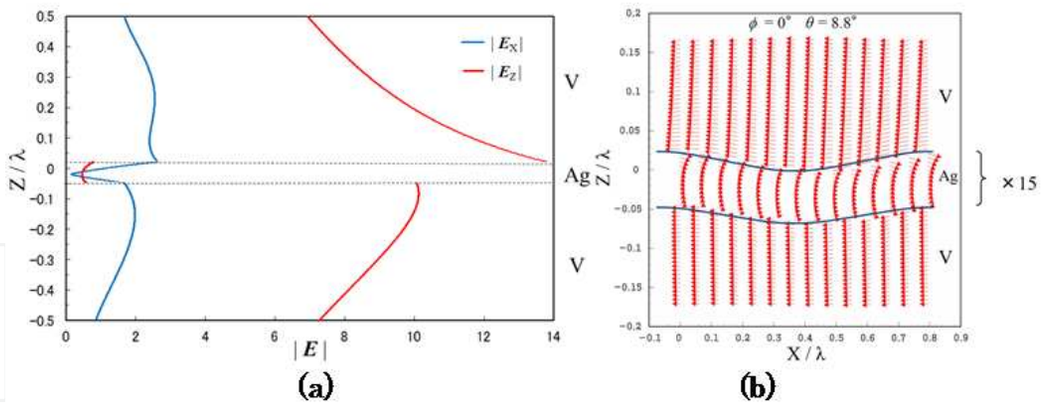

Figure 16. Field distributions (a) and energy flows (b) at $\theta = 8.8^\circ$, which corresponds to the right dip on the $e/d = 0.08$ curve in Fig. 11.

Figures 14, 15, and 16 show the field distributions of the X- and Z-components of the total electric fields (a) and energy flows (b) in the vicinity of the silver-film grating at the incidence angles at which absorption was observed in Fig. 11. The abscissa and ordinate show the magnitude and distance in the Z direction normalized by the wavelength λ. The parallel broken lines represent the grating surfaces.

Figure 14 shows $\boldsymbol{E_X}$ and $\boldsymbol{E_Z}$ (a), Sx and Sz (b) for the case of $e/d = 0.4$ at $\theta = 8.0^\circ$, which corresponds to the single dip in Fig. 11(a). Figures 15 and 16 show the same thing for the $e/d = 0.08$ case. Figure 15 illustrates the results at $\theta = 6.54^\circ$, where the left dip is observed in Fig. 11(a). On the other hand, Fig. 16 depicts the results at $\theta = 8.8^\circ$, corresponding to the right dip in Fig. 11(a). In Figs. 14 to 16, we observe strong enhancement of $\boldsymbol{E_X}$ and $\boldsymbol{E_Z}$ (note that the magnitude of the incident radiation is 1), which is observed at the incidence angles where absorption occurs.

We observed that the total field above the grating surface decays exponentially in the Z direction and the magnitude of the total field is almost E_Z in Fig. 14(a). The state of affairs is nearly the same in the metal region except for the rapid decay. Because the grating is thick, the oscillation near the upper surface does not reach the lower surface and, hence, the field below the grating is zero. Figure 14(b) illustrates the energy flow **S**, which is magnified by 15 in the metal region. We see that the energy flow is almost in the X direction and that it goes in opposite directions in vacuum and in metal. This is commonly observed when a SISP is excited.

In Figs. 15(a) and 16(a), we again see the enhancement of E_X and E_Z on the upper and lower surface of the silver-film grating, respectively. The rate of enhancement in Fig. 15(a) is not as large as that in Fig. 16(a). E_Z is strongly enhanced at both the upper and lower surfaces of the grating and exponentially decays away from each surface. We thus observe the simultaneous excitation of surface plasmons at the surfaces. We can understand the difference of the field distributions assuming that the former and the latter refer to Figs. 15 and 16 are the results of the SRSP and the LRSP mode excitation. Figures 15(b) and 16(b) complement the understanding showing the even and odd nature of relevant oscillations.

4.4. Multilayered thin-film bi-gratings case

Next, we consider multilayered thin-film bi-gratings as shown in Fig. 1(a) indicated by $L = 4$ ($V/Ag/SiO_2/Ag/V$) that consists of a stack of silver and SiO_2 films pairs. As listed in the figure, the values of the parameters are the same as those in Fig. 11 except for $L = 4$, $n_{SiO_2} = 1.5$, $e_{SiO_2} / d = 0.3$ or 0.08 .

4.4.1. Diffraction efficiency

Figure 17 shows the (0,0)th order power reflection ρ_{00} in V_1 (Vacuum) (a) and the transmission coefficient τ_{00} in V_5 (Vacuum) (b) as functions of the incident angle θ for two different values of e_{SiO_2} / d . The curve for $e_{SiO_2} / d = 0.08$ is almost the same as for a sinusoidal silver film bi-grating (Fig. 11): the coupled surface plasmon modes, SRSP and LRSP, are excited. On the other hand, in the curve for $e_{SiO_2} / d = 0.3$, we find a new type of absorption of incident light besides the plasmon resonance absorption associated with SRSP or LRSP.

This is related to the resonant excitation of a guided wave supported by the SiO_2 film. This absorption is characterized by its occurrence over a wider range of θ . For example, in the case of $e_{SiO_2} / d = 0.3$, the extinction power is more than 50% for all angles of incidence θ ranging from 0° to 12° .

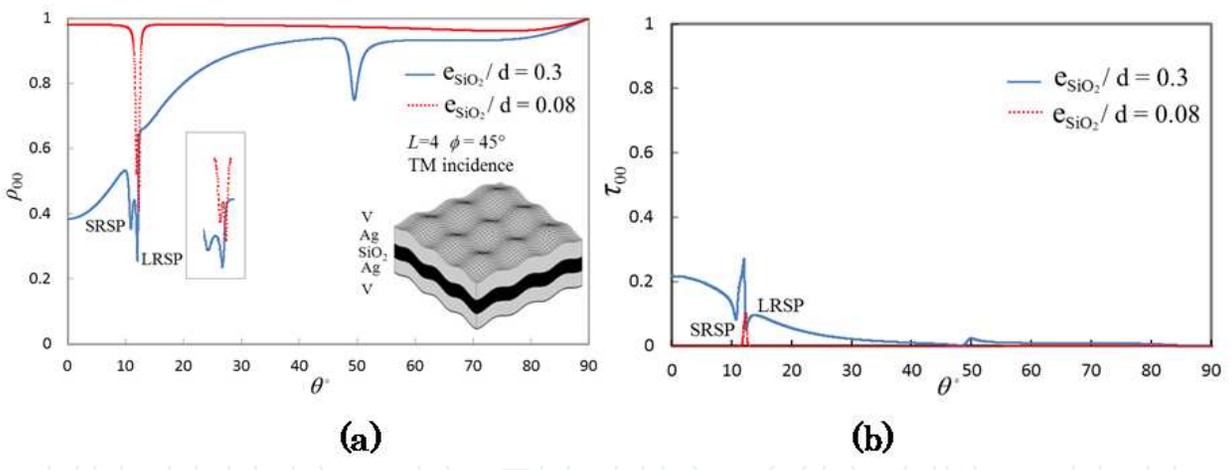

Figure 17. The (0, 0)-th order diffraction efficiencies ρ_{00} (a) and τ_{00} (b) as functions of θ for two values of e_{SiO2}/d (L=4).

4.4.2. Field distributions

In order to examine the properties of the wide absorption found in Fig. 17, we investigated the field distributions of the total electric field E^{total} and the TM component of the (0, 0)th-order diffracted electric field $\boldsymbol{E}^{TM}_{l(0,0)}$ in the vicinity of the SiO_2 film. The magnitude of E^{total} and $E^{TM}_{l(0,0)}$ (l =1,2,...5) along the Z-axis are plotted in Fig. 18 where $\theta = 0^\circ$ and $e_{SiO_2} / d = 0.3$.

We observe in the figure that the field distributions of E^{total} inside the SiO_2 film indicates a standing wave pattern corresponding to the normal mode of a one dimensional cavity resonator, and that the distribution is almost close to that of $E^{\text{TM}}_{3(0,0)}$. Hence, we conclude that the wide absorption observed in the multilayered grating V/Ag/SiO_2/Ag/V is associated with resonance of the (0, 0)th-order diffracted wave $E^{\text{TM}}_{3(0,0)}$ in the SiO_2 film sandwiched by a sinusoidal silver film grating.

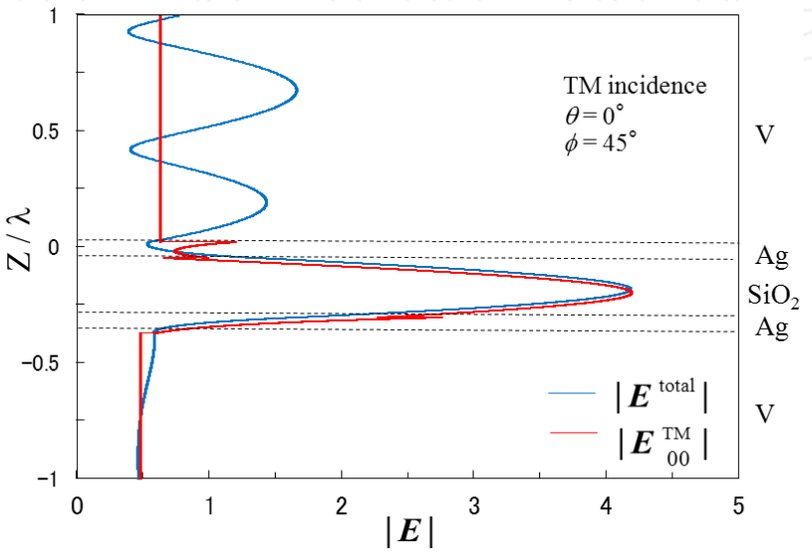

Figure 18. Standing wave pattern of the electric filed in the SiO_2 film.

5. Conclusions

We have investigated the resonance absorption associated with the resonant excitation of surface plasmons in bi-gratings. Calculating diffraction efficiency, expansion coefficients, field profiles, and energy flows, we examined the characteristics of the resonant excitation of surface plasmons in detail. Interesting phenomena were revealed, including the conversion of a TM (or TE) component of the incident light into a TE (or TM) component at several different incidence angles, strong field enhancement on the grating surface where surface plasmons are excited, and simultaneous resonance absorption that does not occur in the case of a singly periodic grating in general. The results presented here facilitate a clear understanding of the coupled plasmon modes, SISP, SRSP and LRSP, excited in a thin film doubly periodic metal grating.

Author details

Taikei Suyama, Akira Matsushima and Yoichi Okuno
Graduate School of Science and Technology, Kumamoto University, Kurokami, Kumamoto, Japan

Toyonori Matsuda
Kumamoto National College of Technology, Suya, Nishigoshi, Japan

Acknowledgement

This work was supported in part by Grant-in-Aid for Scientific Research from Japan Society for the Promotion of Science (Grant number 23560404). The authors thank Shi Bai and Qi Zhao for help in numerical computation and in preparation of the manuscript.

6. References

Raeter, H., (1982) Surface Plasmon and Roughness, *Surface Polaritons*, V. M. Argranovich and D. L. Mills, (Ed.), Chap. 9, 331-403, North-Holland, New York

Nevièr, M., (1980) The Homogenous Problem, *in Electromagnetic Theory of Gratings* R. Petit (Ed.), Chap. 5, 123-157, Springer-Verlag, Berlin

DeGrandpre, M.D., and L.W. Burgess, (1990) Thin film planar waveguide sensor for liquid phase absorbance measurement, *Anal. Chem.*, 62, 2012-2017

Zoran, J. and M. Jovan, (2009) Nanomembrane-Enabled MEMS Sensors: Case of Plasmonic Devices for Chemical and Biological Sensing, *Micro Electronic and Mechanical Systems*, Kenichi Takahata (Ed.), ISBN: 978-953-307-027-8, InTech

Nemetz, A., U. Fernandez and W. Knoll, (1994) Surface plasmon field-enhanced Raman spectroscopy with double gratings, *J. Appl. Phys*, 75, 1582-1585

Barnes,W. L., T. W. Preist, S. C. Kitson, J. R. Sambles, N. P. K. Cotter, and D. J. Nash, (1995) Photonic gaps in the dispersion of surface plasmons on gratings, *Phys. Rev. B*, 51, 11164 -11167

Tan, W.-C., T. W. Preist, J. R. Sambles, M. B. Sobnack, and N. P. Wanstall, (1998) Calculation of photonic band structures of periodic multilayer grating systems by use of a curvilinear coordinate transformation, *J. Opt. Soc. Am. A*, 15, 9, 2365–2372

Inagaki, T., M. Motosuga, E.T. Arakawa and J.P. Goudonnet, (1985) Coupled surface plasmons in periodically corrugated thin silver films, *Phys. Rev. B*, 32, 6238-6245

Chen, Z., I. R. Hooper, and J. R. Sambles, (2008) Strongly coupled surface plasmons on thin shallow metallic gratings, *Phys. Rev. B*, 77, 161405

Bryan-Brown, G.P., S.J. Elston, J.R. Sambles, (1991) Coupled surface plasmons on a silver coated grating, *Opt. Commu.*, 82, No. 1-2, 1-5

Davis, T. J., (2009) Surface plasmon modes in multi-layer thin-films, *Opt. Commu.*, 282, 135-140

Raeter, H., (1977) Surface plasma ocillations and their applications, *Physics of Thin Films*, G. Hass and M.H. Francombe (Ed.), Chap. 9, 145-261, Academic Press, New York

Okuno, Y. and T. Suyama, (2006) Numerical analysis of surface plasmons excited on a thin metal grating, *Journal of Zhejiang University -Science A*, 7, No. 1, 55-70

Suyama, T., Y. Okuno and T. Matsuda, (2009) Plasmon resonance-absorption in a metal grating and its application for refractive-index measurement, *Journal of Electromagnetic Waves and Applications,* 20 , No. 2, 159-168

Chen, Z. and H. J. Simon, (1988) Attenuated total reflection from a layered silver grating with coupled surafce waves, *J. Opt. Soc. Am. B*, 5, No. 7, 1396-1400

Hibbins, A. P., W. A. Murray, J. Tyler, S. Wedge, W. L. Barnes and J. R. Sambles, (2006) Resonant absorption of electromagnetic fields by surface plasmons buried in a multilayered plasmonic nanostructure, *Phys. Rev. B*, 74, 073408

Glass, N. E., A. A. Maradudin and V. Celli, (1982) Surface plasmons on a large-amplitude doubly periodic corrugated surface, *Phys. Rev. B*, 26, 5357-5365

Glass, N. E., A. A. Maradudin, and V. Celli, (1983) Theory of surface-polariton resonances and field enhancements in light scattering from doubly periodic gratings, *J. Opt Soc. Am.*, 73, 1240-1248

Inagaki, T., J. P. Goudonnet, J. W. Little and E. T. Arakawa, (1985) Photoacoustic study of plasmon-resonance absorption in a doubly periodic grating, *J. Opt Soc. Am. B*, 2, 432-439

Harris, J. B., T. W. Preist, J. R. Sambles, R. N. Thorpe and R. A. Watts, (1996) Optical response of doubly periodic gratings, *J. Opt Soc. Am. A*, 13, 2041-2049

Chen, C. C., (1973) Transmission of microwave through perforated flat plates of finite thickness, *IEEE Trans. Microwave Theory Tech.*, MTT-21, 1-6

Yasuura, K. and T. Itakura, (1965) Approximation method for wave functions (I),(II), and (III), *Kyushu Univ. Tech. Rep*, 38, 72-77, 1965; 38, 378-385, 1966; 39, 51-56, 1966

Yasuura, K.(1971). A view of numerical methods in diffraction problems, *Progress in Radio Science 1966-1969*, W. V. Tilson and M. Sauzade (Ed.), 257-270, URSI, Brussels

Okuno, Y., (1990) Mode-matching Method, *Analysis Methods for Electromagnetic Wave Problems*. E. Yamashita (Ed.), 107-138, Artech House, Boston

Hugonin, J. P., R. Petit, and M. Cadilhac, (1981) Plane-wave expansions used to describe the field diffracted by a grating, *J. Opt. Soc. Am.*, 71, No. 5, 593–598

Lawson, C. L. and R. J. Hanson, (1974) Solving Least Squares Problem, Prentice-Hall, Englewood Cliffs, N. J.

Matsuda, T. and Y. Okuno, (1993) A numerical analysis of planewave diffraction from a multilayer-overcoated grating, *IEICE*, J76-C-I, No. 6, 206–214

Matsuda, T. and Y. Okuno, (1996) Numerical evaluation of plane-wave diffraction by a doubly periodic grating, *Radio Sci.*, 31, 1791-1798

Suyama, T., Y. Zhang, Y. Okuno, Z. Q. Luo and T. Matsuda, (2010) Surface Plasmon Resonance Absorption in a Multilayered Bigrating, *PIERS Online*, 6, No. 1, 76-80

Suyama, T., Y. Okuno, A. Matsushima and M. Ohtsu, (2008) A numerical analysis of stop band characteristics by multilayered dielectric gratings with sinusoidal profile, *Progress In Electromagnetics Research B*, 2, 83-102

Hass, G. and L. Hadley, (1963) Optical properties of metals, *American Institute of Physics Handbook* , D. E. Gray, (2nd Ed.), 6-107, McGraw-Hill, New York.

Elston, S. J., G. P. Bryan-Brown and J. R. Sambles, (1991) Polarisation conversion from diffraction gratings, *Phys. Rev. B*, 44, 6393-6399

Matsuda, T., D. Zhou, and Y. Okuno, (1999) Numerical analysis of TE-TM mode conversion in a metal grating placed in conical mounting, *IEICE C-I*, J82-C-I, No. 2, 42-49 (in Japanese).

Suyama, T., Y. Okuno and T. Matsuda, (2007) Enhancement of TM-TE mode conversion caused by excitation of surface plasmons on a metal grating and its application for refractive index measurement, *Progress In Electromagnetics Research,* 72, 91-103

Ritchie, R. H., E. T. Arakawa, J. J. Cowan and R. N. Hamm, (1968) Surface-plasmon resonance effect in grating diffraction, *Phys. Rev. Lett.*, 21, 1530-1533